electronics

MDPI

Article

Joint Optimization of Configuration Design and Energy Management Strategy for a Fuel Cell/Supercapacitor Rubber Tire Gantry Crane

Pingyuan Wang [1], Jianping Dou [1,*], Pengcheng Yin [2], Zhanghao Ni [1], Zhikang Jiang [1] and Danyang Zhao [2]

[1] School of Mechanical Engineering, Southeast University, Nanjing 211189, China; 230219117@seu.edu.cn (P.W.); 220240367@seu.edu.cn (Z.N.); 220220334@seu.edu.cn (Z.J.)
[2] China Railway Siyuan Survey and Design Group Co., Ltd., Wuhan 430063, China; 004348@crfsdi.com (P.Y.); 006849@crfsdi.com (D.Z.)
* Correspondence: jp.dou@seu.edu.cn

Abstract

A fuel cell (FC)/supercapacitor (SC) hybrid powertrain is proposed for rubber tire gantry (RTG) cranes, aiming to address their characteristics of high peak/low average power demand and huge potential energy recovery. Unlike conventional design methods that neglect the coupling effects of energy management strategies (EMSs), this paper adopts a joint optimization (JO) for the powertrain parameters' design. Parameters are preliminarily sized based on routine container handling tasks, then refined via a dynamic programming (DP)-based EMS for secondary optimization to minimize the total crane operation costs that cover hydrogen consumption as well as FC degradation. Iterations of the optimization process continue until targets are met. The results indicate that the JO framework achieves dual energy-economic goals, exhibiting a 57.33% enhancement in fuel economy compared to diesel-powered cranes through port validation while concurrently decreasing the SC's capacity redundancy by 12.7%. These findings aid FC/SC RTG crane configuration design in ports. Additionally, the theoretical optimal operation cost obtained by the DP-based EMS can be used as a benchmark for evaluating other EMSs.

Keywords: joint optimization; rubber tire gantry crane; fuel cell/supercapacitor; configuration parameters; energy management strategy; dynamic programming

1. Introduction

The growth of maritime logistics, handling over 85% of global cargo, has intensified port emissions. Shipping has become the third largest air pollution source in China [1], motivating vigorous green transition policies under the "dual carbon" goal [2]. Land-side port operations, particularly container handling, contribute substantially to atmospheric pollutant emissions [3]. Notably, diesel-powered rubber tire gantry (DPRTG) cranes are primary emission sources in container operations, with a rated power of more than 400 kW and 14 L/h fuel consumption, yielding the production of 40 kg/h CO_2 [4]. Such conventional cranes can no longer meet modern energy-saving and low-carbon requirements. Moreover, DPRTG cranes suffer from extremely low energy recovery efficiency—merely 15~20% of potential regenerative energy can be recycled during container lowering—resulting in massive energy waste [5].

Various approaches are intended to cut fuel consumption of DPRTG cranes. One cost-efficient solution is to hybridize the powertrain system by utilizing energy storage

Check for updates

Academic Editor: Pablo García Triviño

Received: 30 April 2026
Revised: 19 June 2026
Accepted: 22 June 2026
Published: 25 June 2026

Copyright: © 2026 by the authors. Licensee MDPI, Basel, Switzerland. This article is an open access article distributed under the terms and conditions of the Creative Commons Attribution (CC BY) license.

systems such as supercapacitors (SCs), batteries, or flywheels, either individually or in combination [6–9]. However, these powertrain systems are typically oversized relative to actual operational power demands: many port cranes operate at only 30~50% of their rated power, increasing energy costs by 20~30% due to excessive energy consumption and idle losses. Given the standardized nature of container handling, in-depth investigation into configuration parameters of RTG cranes is essential to improve resource utilization. Meanwhile, energy management strategies (EMSs) are inherently coupled with powertrain component sizing, a relationship widely recognized in marine propulsion and hybrid electric vehicles [10–12], offering a synergistic pathway for the optimal design of RTG systems.

The above statement highlights the following questions needing to be addressed to achieve high efficiency and economic performance of port RTG cranes:

1. What powertrain configuration is suitable for RTG cranes requiring efficient energy recovery?
2. How to optimize the size of the powertrain components for fixed-operation RTG cranes to balance energy efficiency and cost?
3. How to employ EMSs to maximize energy efficiency of RTG cranes and collaboratively optimize configuration parameters?

For RTG cranes, frequent start-stop, substantial regenerative energy, and drastic instantaneous peak power impose stringent performance requirements on the energy storage system. Although lithium-ion batteries are widely used in vehicles and some researchers have investigated their application in RTG cranes [6], they suffer from rapid lifespan degradation under frequent charge–discharge cycles and carry potential risks of thermal runaway after low-temperature cycling [13]. In contrast, SCs feature high power density (>1 kW/kg), long cycle life (>500,000 cycles), good low-temperature performance (−40~+50 °C), and high safety, making them more suitable than lithium-ion batteries to be the energy storage system of RTG cranes [14]. Some researchers have proposed a hybrid powertrain combining a diesel generator (DG) and SC energy storage system [15]. However, it is worth noting that this measure cannot reduce carbon emissions directly. The reduction in port emissions requires a multifaceted approach, including the adoption of cleaner fuel sources and optimization of operational practices. Therefore, this paper proposes a novel fuel cell (FC)/SC hybrid powertrain RTG crane (FCRTG crane) which can achieve near-zero emissions while meeting high-power operation requirements.

Owing to hydrogen's zero-emission attribute and swift refueling capabilities, fuel cell systems (FCSs) have been applied to heavy-duty equipment such as vehicles and trains [16–18]. Since RTG cranes operate along fixed routes and impose low requirements for hydrogen infrastructure, FCs represent a golden solution for the green transition of port cranes. Supported by government subsidies, the capital cost of FCRTG cranes in China has become competitive with that of conventional DPRTG cranes. In 2022, Qingdao Port launched research on hydrogen-powered cranes [19]. As an industry pioneer in hydrogen ports, it also constructed China's first port hydrogen fueling station for port logistics. Globally, integrated ports in the United States, Japan, and Europe are being transformed into hydrogen ports [20]. However, FCs alone cannot satisfy transient high-power demands during startup and lifting, nor can they recover regenerative potential energy during descending and braking [21]. These limitations necessitate a hybrid powertrain system featuring SCs for auxiliary energy supply to achieve high energy density and rapid dynamic response. Given the stable load profiles and fixed operating patterns of RTG cranes, refined powertrain component sizing is critical to avoiding redundant resource allocation and control costs. The high initial investment remains a major barrier to FC/SC hybrid powertrain applications. Thus, configuration optimization is indispensable.

The configuration optimization of powertrain systems is classified into two categories: single and joint optimization (JO). Single optimization only focuses on component parameters and ignores the coupling effect with EMSs [22]. However, the energy-saving performance of a hybrid powertrain system is a multivariate optimization issue closely related to EMSs, operational conditions, and component capacity. JO, while theoretically comprehensive, faces limitations including high-dimensional search space, slow algorithmic convergence, and compromised solution accuracy. To address these challenges, this paper focuses on the hierarchical JO of configuration parameter design and EMS for the powertrain system of FCRTG cranes, aiming to minimize energy consumption and carbon emissions.

EMSs rationally allocate power from multiple energy sources to adapt to fluctuating power demands, effectively reducing fuel consumption. EMSs have been extensively studied in hybrid vehicles [23–26], rail coaches [27,28], tractors [29–31], and power grids [32–34]. Common EMSs include rule-based (deterministic rules, fuzzy rules) and optimization-based strategies (model predictive control (MPC), genetic algorithms (GAs), dynamic programming (DP), and Pontryagin's minimum principle (PMP)). Table 1 summarizes existing research on EMSs and configuration design of different equipment from the literature, with their characteristics.

Table 1. Research on EMSs and configuration design in the literature.

Equipment	Authors	EMSs	Configuration	JO
Vehicles	Ferrara et al. [10]	DP	FC+battery	√√
	Shen et al. [11]	Fuzzy control	Battery+SC	×
	Chen et al. [12]	DP+GAs	FC+battery	√
	Jia et al. [24]	Twin delayed deterministic EMS	FC+battery	×
	Tang et al. [25]	Rule-DDPG method	FC+battery	√
	Song et al. [35]	MPC	FC+battery	√
	Gharibeh et al. [36]	A bi-level online EMS	FC+battery	√
	Lü et al. [37]	DP+MPC	Gasoline+battery	√
Rail coaches	Sipra et al. [27]	Fuzzy logic	Solar PV–battery	×
	Xu et al. [28]	Electric–thermal collaborative	FC+heat pump	√
Tractors	Varlese et al. [29]	A predictive EMS	FC+battery	×
	Radrizzani et al. [30]	MPC	ICE	×
Power grid	Haffaf and Lakdja [32]	A multi-stage optimization EMS	PV–battery–ICE	√
	Wang et al. [33]	Fuzzy neural networks and a modified PSO	PV–battery–turbine	×
RTG cranes	Kusakaka et al. [7]	A rule-based EMS	DG+battery	√
	Takalani and Masisi [8]	Filtering and PMP	Battery+SC+grid	×
	Corral-Vega et al. [15]	Voltage control	DG+SC	√
	Takalani and Masisi [38]	A rule-based EMS	Battery+SC+grid	×
	Chen et al. [39]	Game theory	DG+SC+battery	×
	Alasali et al. [40]	GAs	Grid+storage system	×
	Lin et al. [41]	PSO and tabu search	Electric-powered	×

Note: √√ (Deeper study); √ (Simple study); × (No consideration).

As observed in Table 1, while extensive explorations of EMSs target vehicles, rail coaches, and tractors, relevant research on EMSs for RTG cranes integrated with FC and SC remains absent. Notably, RTG cranes differ fundamentally from road vehicles, rail coaches and tractors: they operate under fixed, cyclic working conditions with fewer interfering factors, whereas vehicles are subject to complex and variable road and traffic scenarios [42]. Furthermore, benefiting from their ultra-high load capacity, RTG cranes can store and release considerably more potential energy during lifting operations than conventional

transportation equipment, which endows EMSs with outstanding energy-saving potential in such hoisting machinery. Specifically, existing EMS studies on hybrid RTG cranes mainly focus on optimizing diesel engine performance and partially adopting supercapacitors for potential energy recovery. In view of the promising energy-saving prospects of cranes, several scholars have begun to explore EMSs for various hybrid RTG crane configurations. To the authors' knowledge, however, the overall research on EMSs for hybrid cranes is still very limited. Takalani and Masisi [38] developed a rule-based EMS for distributing output power among the battery, supercapacitor, and grid. Their novel hybrid energy storage system created a decrease in energy consumption and peak power demand for the crane operation. Alasali [43] proposed a deterministic optimal EMS controller and MPC strategy as a feasible solution to minimize the electric expenses linked to dynamic power tariffs and mitigate peak power demand under predefined powertrain parameters and grid constraints.

Nevertheless, most existing EMS studies fail to incorporate JO, as summarized in the last column of Table 1. At the same time, although several studies have discussed the influence of EMSs on crane energy efficiency, the mutual coupling between system configuration design and EMSs has been largely neglected. Accordingly, the research domain of joint optimization focusing on such coupling effects has not been explored so far. In terms of FC/SC hybrid crane systems, preliminary explorations have only been conducted in the broader field of green-energy-driven hoisting equipment. Against this background, this paper proposes a joint optimization framework for FCRTG cranes, with a core focus on the coupling mechanism between configuration design and EMSs.

In the current studies on powertrain system design and EMSs of hybrid RTG cranes, there still exist some gaps requiring urgent attention:

1. Although investigations have been conducted on battery-SC hybrid cranes, the application potential of FCSs remains insufficiently explored, which hinders the development of zero-emission port logistics. Most existing FC-related studies mainly focus merely on vehicles, without considering the high-power output and cyclic operating characteristics unique to RTG cranes.
2. Integrated research that combines practical operational requirements with EMS optimization for RTG powertrain parameter matching is still lacking. The existing parameter design approaches mostly adopt oversimplified principles or directly transplant methodologies from vehicle research, thereby failing to achieve optimal resource utilization and overall system efficiency.
3. The majority of currently developed EMSs for RTG cranes rely on rule-based strategies, which cannot guarantee global optimization performance. Moreover, standardized and benchmark EMS solutions are still absent for RTG cranes operating under fixed-cycle working modes.

As a widely employed global optimization method, DP is adopted to distribute energy among different power sources based on predictive operating cycles. Despite its high demand for computing capacity, DP works well for precomputed analysis including comparing various powertrain architectures, assessing online EMSs, and formulating guidelines for RTG cranes. Under a particular operating cycle, the theoretical minimum value of energy consumption can be derived via DP for port RTG cranes with a determined system structure and steady-state environment. Consequently, DP is employed to address the energy management issues of RTG cranes. The obtained theoretical optimal solutions can serve as benchmarks for other EMSs and be used to guide the optimization of the design parameters of the crane system.

In summary, this paper proposes a JO strategy to address the configuration parameter design of the new powertrain system for RTG cranes. The main contributions of this paper include the following:

1. A dedicated FC/SC architecture for hydrogen-powered RTG cranes is presented, which can store regenerated potential energy and deliver instant kinetic power during acceleration.
2. A DP-based EMS in FCRTG cranes with fixed-cycle heavy lifting scenarios is explored, which establishes a benchmarks for other EMSs.
3. The JO framework achieves dual energy-economic objectives, demonstrating through port validation a 57.33% fuel economy boost while reducing capacity redundancy of the SC by 12.7%.

The subsequent parts of this paper are arranged in the following order. The problem statement and solution framework are detailed in Section 2. Section 3 establishes the powertrain model of the FCRTG crane. The principles and implementation of the DP are explained in Section 4. Four instances are computed in Section 5, along with relevant results comparison and discussion. Finally, the research findings are summarized in Section 6.

2. Problem Statement and Solution Framework

2.1. Problem Statement

In traditional situations, RTG cranes are powered to finish duty cycles by a diesel generator set including a diesel engine coupled with an alternator. The electricity undergoes rectification and is then distributed via a DC network to all motors powering the elevators, carts, and movement systems of the RTG crane. As the container unloads, the electric motor produces electricity and feeds it back into the DC network. Without an energy storage device for recovery, the surplus energy is forced to be dissipated in the resistor bank. However, with adequate energy storage, the excess energy can be retained, retrieved, and utilized during subsequent operations, leading to substantial energy savings, especially considering that RTG cranes often handle hundreds of containers daily. During normal operations, data collected from an RTG crane equipped with suitable instruments can help assess the efficiency of current motor energy consumption and required power under different cycles so that an EMS strategy can be explored.

The notations and their corresponding meanings in this paper are given in Table 2.

Table 2. The notations and their meanings in this paper.

Notations	Meanings	Notations	Meanings
P_{fc}	power of the FC	η_{fc}	the FC efficiency
P_{sc}	power of the SC	η_{sc}	the SC efficiency
η_{fcdc}	efficiency of DC/DC converters connected to the FC	η_{scdc}	efficiency of DC/DC converters connected to the SC
P_t	total power demand of the RTG crane	C_{sc}	capacitance of the SC
$\overline{P}$	average power demand	m_{H_2}	hydrogen fuel consumption
C_{op}	operation cost of the RTG crane	C_{H_2}	equivalent hydrogen consumption cost
C_{fc}	degradation cost of the FCS	ΔV_{fc}	rated voltage drop of a single FCS
p_{H_2}	unit price (CNY/kg) of hydrogen	LHV_{H_2}	hydrogen lower heating value
$\alpha_{on\text{-}off}$	start-stop degradation rate of the FCS	α_{shift}	load-shift degradation rate of the FCS

Table 2. *Cont.*

Notations	Meanings	Notations	Meanings
α_{low}	low-power degradation rate of the FCS	α_{high}	high-power degradation rate of the FCS
N_{cycle}	number of start-stop cycles of the FCS	N_{shift}	number of load changes of the FCS
T_{low}	duration of low-power operation of the FCS	T_{high}	duration of high-power operation of the FCS
SOC	state of charge of the SC	SOC_0	initial SOC
$P_{fc\max}$	maximum power of the FC	$P_{fc\min}$	minimum power of the FC
$P_{sc\max}$	maximum power of the SC	$P_{sc\min}$	minimum power of the SC
$SOC_{\max}$	maximum SOC	$SOC_{\min}$	minimum SOC
$U_{\max}$	maximum voltage of the SC	$U_{\min}$	minimum voltage of the SC
k	discrete moment	I_{sc}	current of the SC
$U_{sc,rate}$	rated voltage of the SC	R_{sc}	resistance of the SC
P_{up}	uplink power	T_{up}	uplink time
P_{down}	downlink power	T_{down}	downlink time
E_{sc}	stored energy of the SC	E_{reg}	regenerative energy
η_{reg}	percentage of regenerative energy	m_{rated}	container weight at rated load
E_{charge}	energy absorbed charging from U to $U_{\max}$	E_{charge}	energy released discharging from U to $U_{\min}$

A conventional RTG crane completes 20 operating cycles in 1 h. The load characteristics of the RTG crane reveal that the ratio of peak power to average power is close to 10:1, making its powertrain system highly suitable for a hybrid power solution. Therefore, it is necessary to redesign the RTG crane powertrain system by combining carbon emissions and energy-saving goals. This paper aims to minimize the operation costs by a designed powertrain system. Unlike common simple machines, RTG cranes have separate motors responsible for the travel of the trolley and gantry, as well as the lifting and lowering of the containers. When the trolley or gantry motors brake or the hoist motor descends, the SC can store energy. Therefore, the FC and SC jointly supply power to satisfy the power demands of the RTG crane as follows:

$$P_t = \eta_{fc}\eta_{fcdc}P_{fc} + \eta_{sc}\eta_{scdc}P_{sc}. \tag{1}$$

For the preliminary design of the configuration parameters, the capacities of the FC (P_{fc}) and SC (C_{sc}) are selected as the decision variables which are to meet the power demands (P_t) of crane operations. The power of the FC P_{fc} and the capacitance of the SC C_{sc} satisfy the following constraints:

$$\begin{cases} P_{fc} \geq \frac{\overline{P}}{\eta_{fc}} \\ C_{sc} \geq \frac{2E_{sc}}{\left(U_{\max}^2 - U_{\min}^2\right)} \end{cases}. \tag{2}$$

Simply meeting the aforementioned requirements is insufficient, because the operation cost achieved thereby is not at an optimal level, necessitating secondary optimization via EMSs. In the formulation of the EMS, the main focus is on optimizing the power allocation of the two energy sources to obtain the optimal operation cost. At each time step, the power of the SC P_{sc} is chosen as the decision variable to achieve power distribution, while the state of charge (SOC) of the SC is selected as the state variable. Additionally, the operation cost C_{op} is chosen to be the objective function. The output power of the FC and SC are

restricted by their inherent capacity limits. Furthermore, the SOC is confined between its initial state and the lower bound. The corresponding constraints are concluded as below:

$$\begin{cases} P_{fc\min} \le P_{fc} \le P_{fc\max} \\ P_{sc\min} \le P_{sc} \le P_{sc\max} \\ \mathrm{SOC}_{\min} \le \mathrm{SOC} \le \mathrm{SOC}_{\max} \end{cases}. \tag{3}$$

The total operation cost encompasses the hydrogen consumption cost and the FC degradation cost, as formulated below:

$$J = \min C_{op} = \min\left(C_{H_2} + C_{fc}\right) = \min \sum_{k=1}^{N} L(\mathrm{SOC}(k), P_{sc}(k)). \tag{4}$$

The configuration design of the powertrain system and the specific steps of the DP-based EMS are introduced in detail in Sections 3 and 4. To achieve the dual goals of the JO, the following assumptions are established:

1. The FC operates at an ideal thermal condition and a fixed moisture level, so the model excludes the air cooler and humidifier.
2. The FC and SC in the powertrain are actually composed of multiple units. For the convenience of modeling, they are both treated as an independent structure in this paper.
3. The design of powertrain system parameters is aimed at RTG cranes operating typical loads of containers. If the load changes, the parameters need to be recalculated.

2.2. Solution Framework

A JO of a powertrain system and EMS for the configuration of parameter designs of RTG cranes is proposed. The designed capacity parameters are supposed to minimize operation cost by the DP-based EMS while meeting the power demands of RTG cranes. Considering the inputs, outputs, operating mechanisms, and constraints of the problem, an IDEF0 chart is created in Figure 1. As shown in Figure 1, the optimal result of an EMS is one highly sensitive to the given configuration parameters. On the other hand, to optimize capacity planning and eliminate resource redundancy, the impact of the given EMS on system configuration design must be carefully evaluated by considering operation cost and power allocation.

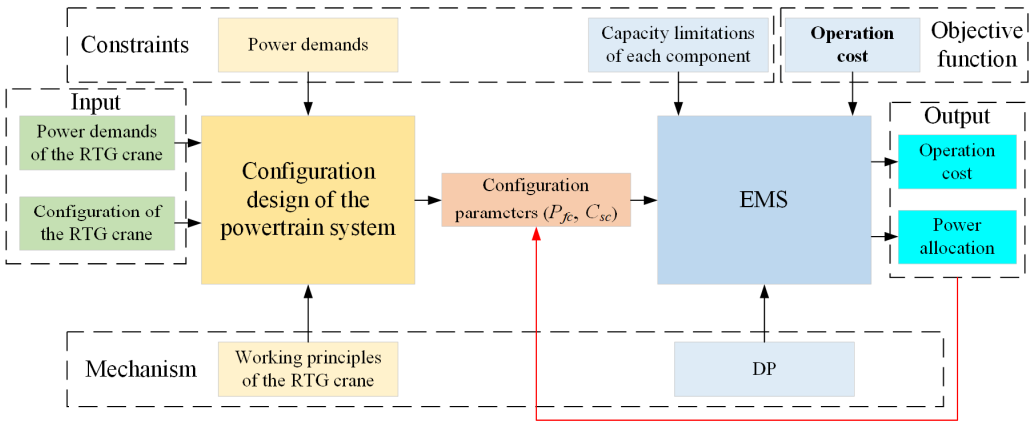


Figure 1. The IDEF0 chart for the JO.

First, a configuration of the crane powertrain is designed, and models of key components are established. Then, the preliminary capacity parameters are tailored to meet the power demands of the RTG crane. Next, a DP-based EMS is utilized to tackle the

JO problem of the configuration design, accounting for the operation cost. In this stage, operation costs quantify the economic benefit of the EMS. Finally, it is essential to verify whether the designed configuration parameters can fulfill the power demands of the RTG crane in the port. If the power demands of the RTG crane cannot be met, the parameters must be updated, even if this ends up compromising the energy-economic goals to some extent. The power demands of the RTG crane comprise the total power demands along with the instantaneous power demand, especially the highest power demand required during startup or acceleration. In the initial design of powertrain parameters, in addition to considering the power demands of the RTG crane, the FC- and SC-related technical specifications were also taken into account. Of course, these values are relatively large and will be further optimized by the EMS to realize cost reduction and lower carbon emissions. Meanwhile, in the process of EMS secondary optimization, the optimal powertrain size with minimal operational cost is sought to avoid capacity redundancy and reduce powertrain size. The main objective of the secondary optimization is operational cost, but the optimized parameters may not meet the high instantaneous power demands and need to be iteratively optimized again. For example, if the parameters of the powertrain system are too small to meet power demands, which perform well in the EMS, this may prevent the RTG crane from working properly. Although the powertrain system has lower operational cost, because of this, it will still be abandoned during the second optimization process.

3. Powertrain System Design

The schematic layout and powertrain system of the FCRTG crane in this paper are designed as illustrated in Figure 2. Figure 2a provides a lateral view drawing corresponding to the practical structure layout of the RTG crane. The FC and SC are integrated and linked to the DC bus via the DC/DC converters, respectively, as shown in Figure 2b. The DC/DC converters serve to regulate the voltage level of the electrical energy flowing from the FC and SC to match the requirements of the DC bus system. To achieve this control, two PI controllers are employed in a cascade configuration. In the yard of the port, it is imperative that the RTG crane remains operational at all times. Consequently, even when the SC is completely discharged, the RTG crane must be capable of handling the container. Based on this requirement, the FC has been designed to produce sufficient power and charge the SC when conditions permit.

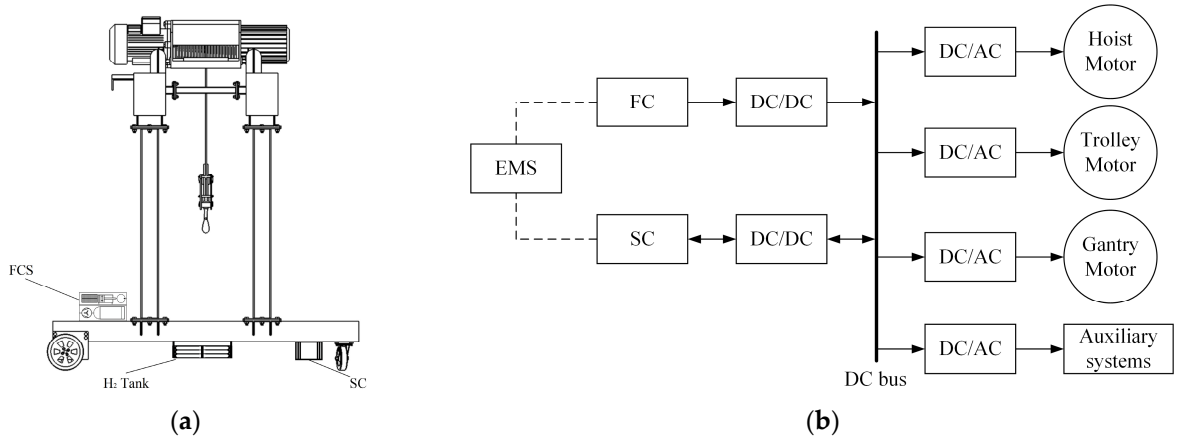


Figure 2. The layout and powertrain system of the RTG crane: (**a**) layout; (**b**) powertrain system.

3.1. Fuel Cell

Among various types of FCs, proton exchange membrane FCs (PEMFCs) represent a favorable choice for transport applications owing to their high power density, specific power output, and relatively low operating temperature [44], which collectively enhance

efficiency and enable rapid system startup. When applied in port scenarios, the FC delivers higher energy efficiency than traditional internal combustion engines throughout the entire energy conversion process [45]. Since the hydrogen tank of the RTG crane can only hold a limited volume of hydrogen, hydrogen consumption is a crucial assessment metric. The following equation quantifies the transient hydrogen consumption rate [46]:

$$\dot{m}_{H_2} = \frac{P_{fc}}{\eta_{fc} LHV_{H_2}}, \tag{5}$$

where $LHV_{H_2} = 120\text{MJ/kg}$ is the lower heating value of hydrogen. Therefore, total hydrogen consumption is determined by integrating its consumption rate over time, calculated as outlined below:

$$m_{H_2} = \int_0^T \frac{P_{fc}}{\eta_{fc} LHV_{H_2}} dt. \tag{6}$$

Thus, the hydrogen consumption cost during the operating cycle of the RTG crane can be computed as follows:

$$C_{H_2} = p_{H_2} \cdot m_{H_2}. \tag{7}$$

Start-stop cycles, variable load transitions, as well as low-power and high-power working states are four typical operating conditions contributing to FC degradation [47]. The established FCS degradation model uses the corresponding degradation rates to faithfully emulate the practical aging progression. The mathematical formula for describing this degradation mechanism is expressed as:

$$\Delta V_{fc} = \alpha_{on\text{-}off} N_{cycle} + \alpha_{shift} N_{shift} + \alpha_{low} \frac{T_{low}}{3600} + \alpha_{high} \frac{T_{high}}{3600}, \tag{8}$$

where ΔV_{fc} denotes the rated voltage drop of a single FC. $\alpha_{on\text{-}off}$, α_{shift}, α_{low}, and α_{high} represent the degradation rates corresponding to the above four operating conditions, respectively. N_{cycle} and N_{shift} stand for the number of start-stop cycles and load changes, respectively. T_{low} and T_{high} represent the durations of low-power and high-power operations, respectively. The relevant degradation rate parameters [48] are summarized in Table 3. The FCS degradation cost can be computed as:

$$C_{fc} = \int_0^t \frac{\Delta V_{fc}}{0.1} \cdot \frac{P_{fc}}{1000} \cdot p_{fcs} dt. \tag{9}$$

Table 3. Degradation rates under different operating conditions in the FCS.

Operating Conditions	Decay Rates	Operating Conditions	Decay Rates
$\alpha_{on\text{-}off}$	13.79 μV/cycle	α_{low}	10 μV/h
α_{shift}	0.0441 μV/kW	α_{high}	8.66 μV/h

3.2. Supercapacitor

As the energy storage component, SC consists of series and parallel connections of single cells. The SC is modeled using an equivalent circuit, similar to that of a battery model, and its key parameters can be expressed as follows [49]:

$$\begin{cases} \text{SOC} = \text{SOC}_0 - \dfrac{\int I_{sc} dt}{C_{sc} U_{sc,rate}} \\ I_{sc} = \dfrac{U_{sc} - \sqrt{U_{sc}^2 - 4 R_{sc} P_{sc}}}{2 R_{sc}} \end{cases}. \tag{10}$$

The fluctuating power demands of RTG cranes lead to continuous changes in the output of the FC and SC. Since the SOC correlates with the real-time power of the SC, its rate is defined as follows:

$$\dot{\mathrm{SOC}} = \begin{cases} -\dfrac{P_{sc}\eta_{sc}}{C_{sc}U_{sc}}, & \text{for charging } (P_{sc} < 0) \\ -\dfrac{P_{sc}}{\eta_{sc}C_{sc}U_{sc}}, & \text{for discharging } (P_{sc} \geq 0) \end{cases}. \tag{11}$$

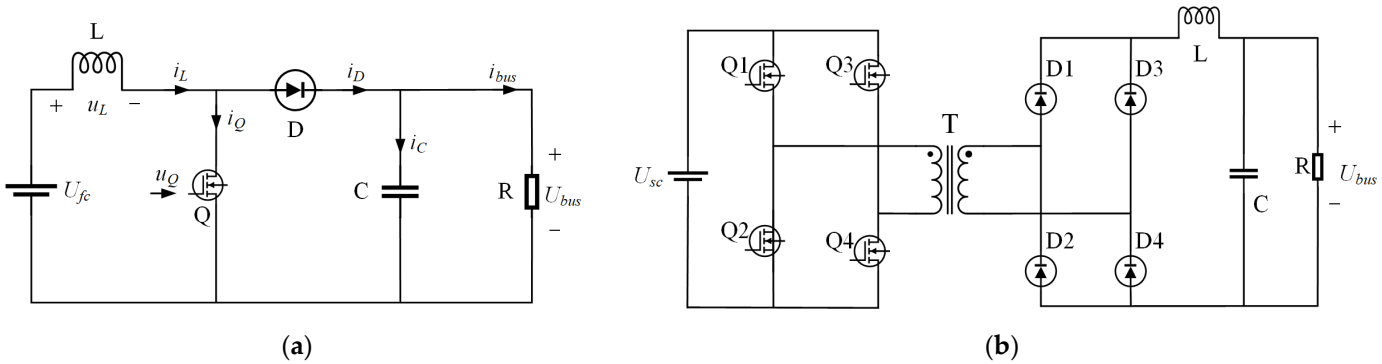
In line with the charging and discharging modes of the SC, equivalent hydrogen consumption is discussed in two cases as follows:

$$m_{H_2} = \begin{cases} \left(\dfrac{P_{fc}}{\eta_{fc}} + P_{sc}\eta_{sc}\right)\dfrac{\Delta t}{LHV_{H_2}}, & \text{for charging } (P_{sc} < 0) \\ \left(\dfrac{P_{fc}}{\eta_{fc}} + \dfrac{P_{sc}}{\eta_{sc}}\right)\dfrac{\Delta t}{LHV_{H_2}}, & \text{for discharging } (P_{sc} \geq 0) \end{cases}. \tag{12}$$

3.3. DC/DC Converters

The terminal voltages of the FC and SC are contingent upon the power exchanged between the two energy units and the DC bus voltage. Consequently, DC/DC converters are necessary to adjust the terminal voltages of the two units to match the DC bus and manage their delivered power.

A unidirectional boost DC/DC converter [50], typically composed of a fully controlled device Q, a power diode D, an energy storage inductor L, and a filter capacitor C, is employed for the FC connecting to the DC bus. The internal circuit structure is shown in Figure 3a. Let the switching period of Q be T_s. In each cycle, its on-time is T_{on} and off-time $T_{off} = T_s - T_{on}$. The duty cycle of drive signal u_Q is T_{on}/T_s. During a switching cycle, the working process of the converter is divided into two states, and the corresponding equivalent circuit diagrams are shown in Figure A1 of Appendix A. As shown in Figure A1a, while the switch Q is conductive during $0 \sim T_{on}$, the diode D bears reverse voltage and remains off. At this moment, U_{fc}, L, and Q form a closed loop, and L stores energy. As shown in Figure A1b, Q turns off during $T_{on} \sim T_s$. The inductor current i_L freewheels through the conducting diode D to form the loop. A new cycle starts at $t = T_s$. The voltage gain of the boost DC/DC converter depends on the duty cycle, denoted as $T_s/(T_s - T_{on})$. The output voltage can be regulated by controlling the duty cycle of Q. The voltage and current waveforms are presented in Figure A2 (T_{on}/T_s = 40%) through simulation in Simulink. Under steady-state operation, all physical quantities are closely related to the duty cycle. The waveform of output voltage clearly illustrates the gain characteristic of the boost converter.



(**a**) (**b**)

Figure 3. The topologies of DC/DC converters: (**a**) unidirectional boost DC/DC converter; (**b**) bidirectional full-bridge isolated converter.

On the other hand, a bidirectional full-bridge DC/DC converter is employed for the SC to facilitate power transfer both from the SC to the DC bus and vice versa. The circuit of the converter is shown in Figure 3b, which consists of four MOSFETs and four diodes. Within one switching cycle, the converter undergoes four states: Q1 and Q4 turned on, all MOSFETs turned off, Q2 and Q3 turned on, and all MOSFETs turned off again, as illustrated in Figure A3. The simulated voltage and current waveforms are presented in Figure A4. For the high-frequency transformer, the two terminals of its primary winding are connected to the midpoints of the left bridge leg (Q1, Q2) and the right bridge leg (Q3, Q4), respectively. The output voltage can be regulated by adjusting the duty cycle of the four MOSFETs. State (a), corresponding to the interval t_0~t_1 and shown in Figure A3a: Q1 and Q4 receive drive signals and turn on. The input voltage is applied across the primary winding. Based on the dot polarity of the transformer windings, D1 and D4 are forward-biased and conduct. The inductor current i_L flows through the secondary winding, diodes D1 and D4, output filter capacitor C, and load resistor R, and rises linearly during this period. State (b), corresponding to the interval t_1~t_2 (Figure A3b): All four MOSFETs Q1–Q4 are switched off, and the primary winding current drops to zero. The inductor freewheels through the four diodes D1 and D4, D2 and D3, with each diode carrying half of the inductor current. The inductor current decreases linearly. State (c), corresponding to the interval t_2~t_3 (Figure A3c): Q2 and Q3 are triggered and turned on. The input voltage is applied across the primary winding again. According to the winding dot convention, D2 and D3 become forward-biased and conduct. The inductor current passes through the secondary winding, D2 and D3, filter capacitor C, and load R, rising linearly once more. State (d), corresponding to the interval t_3~t_4 (Figure A3d), exhibits identical operating characteristics to State (b). The bidirectional converter can control the SC's output and minimize fluctuations in the DC bus voltage, thereby enhancing system stability. Among all isolated DC/DC converters using power devices with identical voltage and current ratings, the full-bridge topology achieves the highest power rating. Therefore, it is widely adopted in medium–high-power industrial power supplies.

3.4. Initial Design Optimization

Given the known cyclic operating conditions of the RTG crane, the power of the FC should meet the demand for average power, which is calculated as follows [51]:

$$\overline{P} = \max\left(\frac{\int P_{up}dt}{T_{up}}, \frac{\int P_{down}dt}{T_{down}}\right). \tag{13}$$

In the hybrid powertrain system, the output power of the SC must satisfy the maximum power demands during crane acceleration and container lifting, while its energy storage capacity should match the maximum recoverable energy during container lowering. Considering extreme operational scenarios, the SC energy configuration should be engineered to accommodate the maximum regenerative energy recoverable from the hybrid powertrain system during rated load conditions:

$$E_{reg} = \eta_{reg} m_{rated} g h. \tag{14}$$

During the charge–discharge process of the SC, energy is expressed as follows:

$$\begin{cases} E_{charge} = \frac{1}{2} C_{sc} \left| U^2 - U_{\max}^2 \right| \\ E_{discharge} = \frac{1}{2} C_{sc} \left| U^2 - U_{\min}^2 \right| \end{cases}. \tag{15}$$

In this paper, $U_{\max}$ = 660 V and $U_{\min}$ = 350 V, since SCs can obtain good charging and discharging effects when operating between 350 V and 660 V, which are determined by [52] and Maxwell technical manuals. A 40-foot container with a lifting height of 18.1 m and a rated load of 30.48 t is considered. In addition to considering the power demands of the RTG crane, the FC- and SC-related technical specifications were also taken into account. Table 4 lists the initial design values of primary parameters of the FCRTG crane. Of course, these values are relatively large and will be further optimized by the EMS to meet the goals of reducing costs and carbon emissions. The hybrid system integrates the commercial brand Maxwell SC with a bidirectional DC/DC converter. During the entire operating cycle (EOC), the container undergoes hoisting, movement, lowering, and unloading at the designated position, culminating in the crane trolley being lifted, shifted, and then lowered back to its idle stance.

Table 4. The initial values of primary parameters of the FCRTG crane.

Component	Parameter	Value
FC	$P_{fc\max}$	80 kW
	$P_{fc\min}$	0
	η_{fc}	0.51~0.57
SC	$P_{sc\max}$	300 kW
	$P_{sc\min}$	−90 kW
	C_{sc}	63 F
	η_{sc}	0.97
	$\mathrm{SOC}_{\max}$	0.9
	$\mathrm{SOC}_{\min}$	0.3
DC/DC converter	η_{fcdc}/η_{scdc}	0.93

4. A DP-Based EMS

In this section, a DP-based EMS for secondary optimization of the RTG crane configuration design is proposed. As a globally recognized optimization algorithm, DP handles multi-source energy distribution efficiently within a specific operating cycle. In this paper, the DP-based EMS is established to find the theoretically best control solution for minimal operation costs and compare the performance of different configuration parameter values for the FCRTG crane. As a comprehensive analysis of DP applications for heavy-duty trucks has been presented in our prior research [3], the principle of DP is not elaborated in this paper.

The operating procedures for the DP-based EMS are as follows:

1. Split the overall multi-stage decision task into multiple independent single-stage subtasks.
2. The SOC of the SC is selected as the state variable and then discretized. The state transition formula is derived from the SC model and presented below:

$$\mathrm{SoC}(k+1) = \begin{cases} \mathrm{SoC}(k) - \dfrac{P_{sc}(k)\Delta t}{\eta_{sc} C_{sc} U_{sc}}, & \text{if } P_{sc} \geq 0 \\ \mathrm{SoC}(k) - \dfrac{P_{sc}(k)\eta_{sc}\Delta t}{C_{sc} U_{sc}}, & \text{if } P_{sc} < 0 \end{cases}. \tag{16}$$

3. Select the SC power Psc as the decision variable.
4. Establish the operation cost as the objective function. All states across each phase come with a certain operation cost, which is computed by Equation (4). Within the interval between time step k to $k+1$, C_{op} takes both equivalent hydrogen consumption

and degradation cost of the FCS into account. Here, L stands for the transition cost function:

$$L = C_{op} = \begin{cases} \left(\dfrac{P_{fc}(k)}{\eta_{fc}} + P_{sc}(k)\eta_{sc} \right) \dfrac{\Delta t}{LHV_{H_2}} \cdot p_{H_2} + \dfrac{\Delta V_{fc}}{0.1} \cdot \dfrac{P_{fc}}{1000} \cdot p_{fcs}, & P_{sc} < 0 \\ \left(\dfrac{P_{fc}(k)}{\eta_{fc}} + \dfrac{P_{sc}(k)}{\eta_{sc}} \right) \dfrac{\Delta t}{LHV_{H_2}} \cdot p_{H_2} + \dfrac{\Delta V_{fc}}{0.1} \cdot \dfrac{P_{fc}}{1000} \cdot p_{fcs}, & P_{sc} \geq 0 \end{cases} . \quad (17)$$

5. Set up the boundary conditions as shown in Equation (3).
6. Iterate to derive the results.

To sum up, the flowchart of DP is presented in Figure 4. *N*S* is the total number of nodes, corresponding to time samples and selected states, respectively. In this paper, the time interval is set to 1 s and S is 6001, which means that the state variable is recursively calculated between 0.3 and 0.9 at 0.0001.

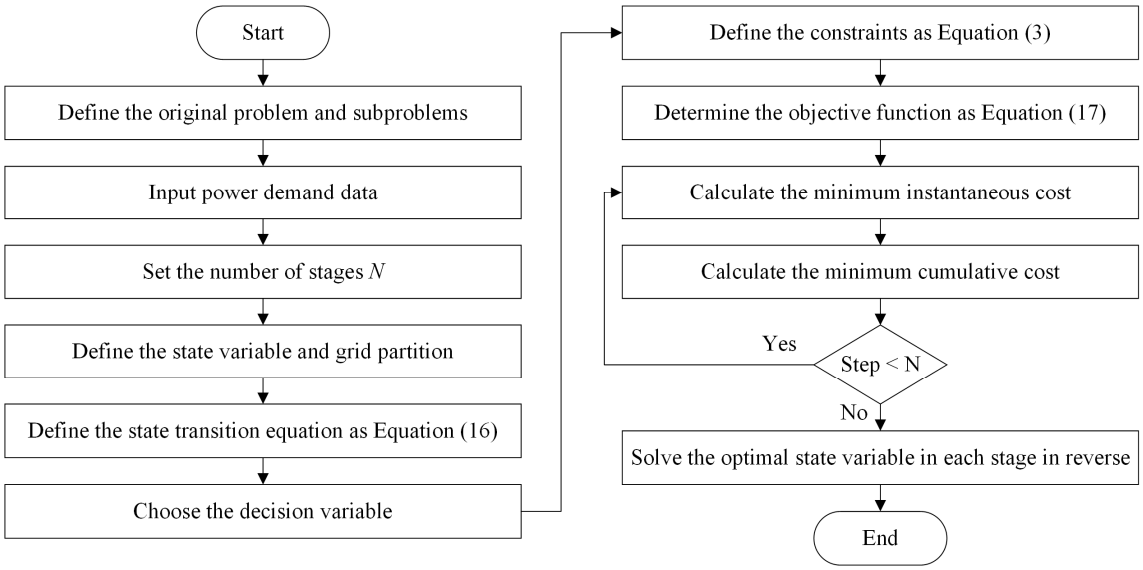


Figure 4. The flowchart of DP.

5. Computational Study

5.1. Design of Experiments

To comprehensively evaluate parameter design and EMSs, three operationally representative cycles are considered in the experiment design. The three operational cycles are an EOC [52] (this reference discusses design, modeling, and control of hybrid cranes in sequence, while ignoring the impact of EMS on power system design and not considering the JO of configuration design and EMS) and two representative work cycles, loading and unloading. Four instances grounded on these three cycles are executed to showcase the advantages of the FC/SC hybrid powertrain, explore the coupling effect between key parameters and EMSs, and perform the JO on configuration parameters of the powertrain system. The attributes of those four instances are listed in Table 5. A comparative study is conducted with three optimization methods. DP, GAs, and a rule-based EMS are employed to address parameter design and energy management of the FCRTG crane.

Table 5. The attributes of the four instances.

Instances	Operating Cycles	Purpose
1	EOC	Demonstrate superiority of DP and FC/SC powertrain
2	EOC	Perform the JO on configuration parameters
3	Loading/unloading	Verify the applicability of the new FC/SC powertrain system
4	EOC	Investigate the operation cost in various working scenarios

Table 4 presents the primary parameters of the RTG crane for instance 1. In instance 2, the influence of RTG crane configuration parameters on the performance characteristics of different EMSs is systematically investigated. To this end, a series of RTG cranes with different parameters are experimentally evaluated using both DP and GA methods. This instance is grounded on the EOC, and Table 6 outlines several key RTG crane parameters. The results of this instance can be used for secondary optimization of the configuration parameters. The novel hybrid powertrain system of the FCRTG crane, which has been secondary optimized, is used in instance 3 to verify its applicability. A series of load profiles are configured in instance 4 for analyzing the performance of the FCRTG crane under heavy loads. As stated in Section 2, the load variations are directly discernible through changes in power demands, with elevated loads resulting in proportionally higher power demands. In this instance, increases of 5% and 10% respectively are applied to the original power demands to evaluate the performance of the EMSs under high-load scenarios. Table 7 provides detailed information regarding these adjustments.

Table 6. Multiple types of configuration parameter values for FCRTG cranes in instance 2.

Number	$P_{fc\max}$/kW	C_{sc}/F	$P_{sc\max}$/kW
P1	60	55	260
P2	80	55	260
P3	60	63	300
P4	60	63	260
P5	80	63	300
P6	40	43	200

Table 7. Different heavy-load working scenarios in instance 4.

Number	Percentage Increase/%	P_{total}/kW
H1	/	1387.86
H2	5	1457.25
H3	10	1526.65

5.2. Analysis of Computational Results

In this paper, all algorithms were coded in Matlab R2022a and run on a PC with 16 GB memory and AMD R7 5800H processor with Radeon Graphics 3.20 GHz. Ten runs were conducted for each operation and instance to obtain average values.

The results obtained by DP under the EOC, alongside the findings that employ GAs and rule-based strategy [52] respectively, are presented in Table 8, and indicate that DP reduces operational cost by 5.47% and 12.50% compared to GAs and rule-based strategy, respectively. Specifically, DP reduces hydrogen consumption by 3.97% and 8.82% compared to GAs and rule-based strategy, respectively. DP can achieve the theoretical minimum hydrogen consumption and can be used to evaluate the effectiveness of different EMSs.

At the same time, since the FCS operates at a relatively high power with fewer load shifts under DP, its degradation cost is lower than that of the other two methods. In addition, the costs of FCRTG and DPRTG cranes are compared. Currently, the hydrogen price stands at CNY 30/kg in China, resulting in a cost of CNY 2.33 for the RTG crane using DP and CNY 2.42 for cranes employing GAs. In contrast, a DPRTG crane requires 0.83 L to complete the EOC, costing CNY 5.98 given the current diesel price of CNY 8.3/L in China. Evidently, FCRTG cranes offer not only zero emissions but also cost savings of over half compared to DPRTG cranes. Although the integration of FCs and SCs leads to a higher initial investment cost, the costs associated with hydrogen production, storage, and transportation are decreasing as FCs gain traction in various countries. An optimized hydrogen energy supply chain can be established through precise planning of the spatial distribution of hydrogen sources and demand sides, and integrating multiple transportation methods including liquid hydrogen tanker trucks, organic hydrogen storage systems, and upgraded pipeline networks [53]. It is particularly important to emphasize that with the implementation of policies and the increase in the penetration rate of the FC market, the overall economy of the hydrogen energy industry chain will experience a qualitative leap in long-distance and large-scale application scenarios. Practical cases from Qingdao Port and Shanghai Port in China demonstrate that the construction costs of hydrogen energy infrastructure are being amortized as hydrogen refueling stations expand in scale [54]. It is anticipated that the retail price of hydrogen will stabilize below CNY 20 per kilogram, further widening the cost advantages of FCRTG cranes. Additionally, hydrogen refueling stations, crucial for the commercialization of hydrogen energy transportation, have undergone rapid development in recent times. China has constructed over 400 hydrogen stations, positioning itself as the global leader. Consequently, when considering the environment, cost, and convenience, the FCRTG cranes proposed in this paper are highly likely to emerge as the ultimate solution for future container handling and loading/unloading in ports. The findings reveal obvious advantages of DP and GAs over the rule-based EMSs. Therefore, subsequent analysis is dedicated to these two algorithms for additional verification of secondary optimization.

Table 8. Fuel consumption and operational cost of different strategies.

EMSs	DP	GA	Rule-Based	DPRTG
Fuel consumption	**0.0775 kg**	0.0807 kg	0.085 kg	0.83 L
Equivalent hydrogen cost (CNY)	**2.33**	2.42	2.55	6.89
Degradation cost of the FCS (CNY)	**0.61**	0.69	0.81	/
Total operation cost (CNY)	**2.94**	3.11	3.36	6.89

Note: The best results are highlighted in bold.

Figure 5 depicts the SOC variation in the SC based on DP and GAs during the EOC. Analogously, simulated data further confirm the prominent superiority of DP against GAs. The curve in Figure 5 indicates a 1.84% decline in the SC SOC within 1 cycle by GA. Notably, the SC SOC returns to its initial value of 0.9 after 88 s by DP due to continuous decline and braking. The SC alternates between persistent charge and discharge by GAs, while the SC primarily discharges with sporadic brief charging periods by DP. This suggests that DP could potentially prolong the SC's lifespan due to reduced charging and discharging cycles. Furthermore, when the container descends (40~52 s), the enormous gravitational potential energy rapidly charges the SC, providing power for subsequent operations and further reducing hydrogen consumption.

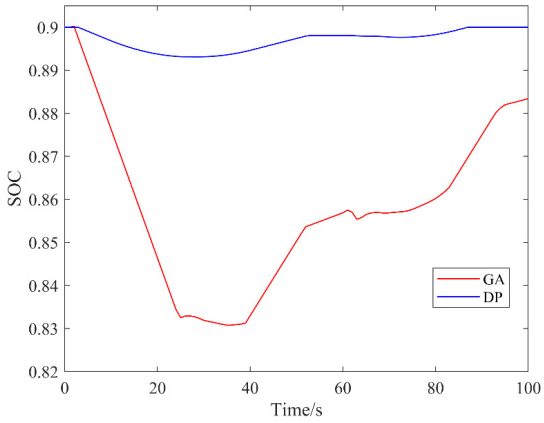
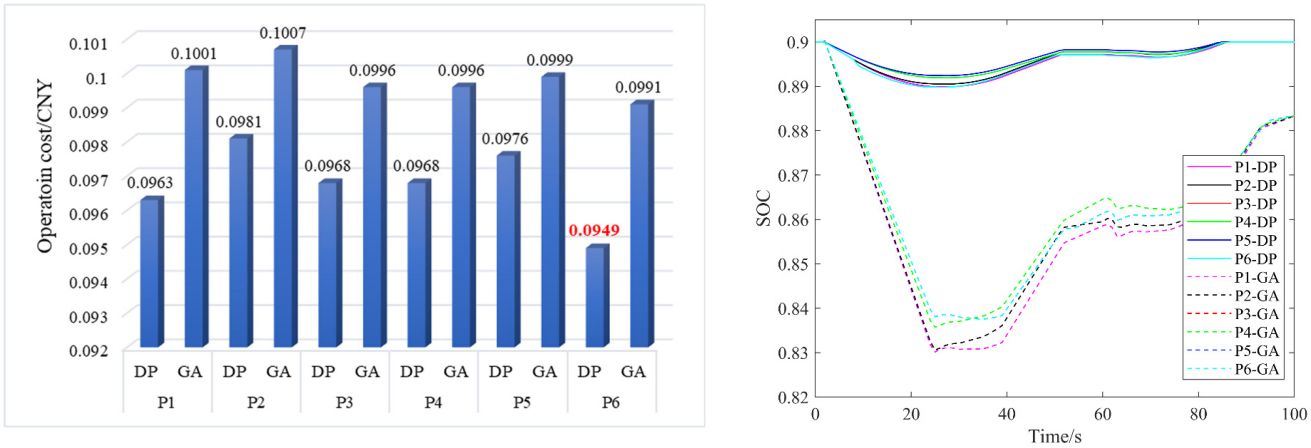


Figure 5. SOC variations during the EOC based on DP and GA.

The operational cost and variation in the SOC of the FCRTG crane across various parameters are illustrated in Figure 6. The operational cost under P6 when using a DP-based EMS is the lowest among all scenarios, attributed to the smallest values of $P_{fc\max}$ and C_{sc}, according to the results in Figure 6a. However, the configuration cannot meet the power demands (as discussed in Section 3.4, the gap from the maximum instantaneous power is approximately 40 kW under EOC conditions), so this optimized design is not feasible. Thus, the values of P1 are chosen for the subsequent instances, resulting in suboptimal operation cost. Additionally, it is evident that variations in $P_{sc\max}$ do not influence operation cost. As the frequency of start-stops increases, a noticeable upward trend in operation cost is observed. Figure 6b depicts the SOC variation curves by DP and GA. In identical conditions, the DP-based SOC fluctuations are comparatively smaller than those observed with GAs. Notably, the SOC under P5 exhibits the highest stability, potentially attributed to the values of $P_{fc\max}$ and C_{sc}. Conversely, the curves corresponding to P3 and P4 align consistently. Figure 6b underscores that higher values of $P_{fc\max}$ and C_{sc} contribute positively to maintaining SOC stability, while $P_{sc\max}$ has no discernible influence on the SOC. This study prioritizes capacity configuration optimization, with the impact of SOC being deemed negligible. The initial design parameters are sufficient to cover the power demands of the RTG crane, thereby reducing the parameter specifications as P1 to avoid capacity redundancy and resource waste.



(**a**) (**b**)

Figure 6. The operation cost (CNY) and variation in the SC SOC by DP and GA under different configuration parameter conditions (The red font denotes the best results): (**a**) operation cost (CNY); (**b**) variation in SOC.

The parameter values in P1 are applied in the following instances. The results show that the hybrid powertrain system designed with secondary optimization is suitable for typical loading/unloading operations. From Figure 7, operation costs are 0.0501 and 0.0521 under loading and unloading operations respectively, decreased by 5.11% and 7.25% compared with GAs in one cycle. To a certain degree, merely comparing the performance of these strategies within a single cycle lacks significance. Hence, the method was cycled to encompass a 1 h operational task with 36 cycles. The results showed reductions of 3.84% and 5.50% for loading and unloading operations, respectively. Additionally, it is worth noting that DP performs better in unloading operations compared to loading ones, due to the higher power demands. Consequently, EMSs based on DP are well-suited for the tasks of heavy-duty port RTG cranes, owing to their broader operational range and duration.

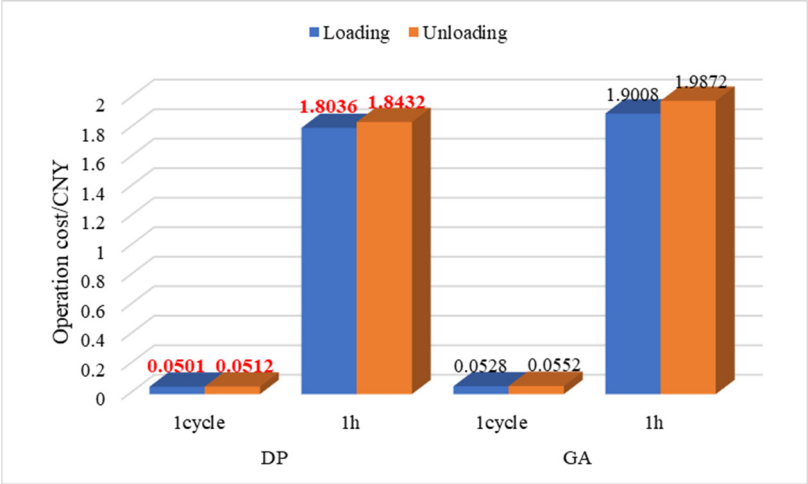
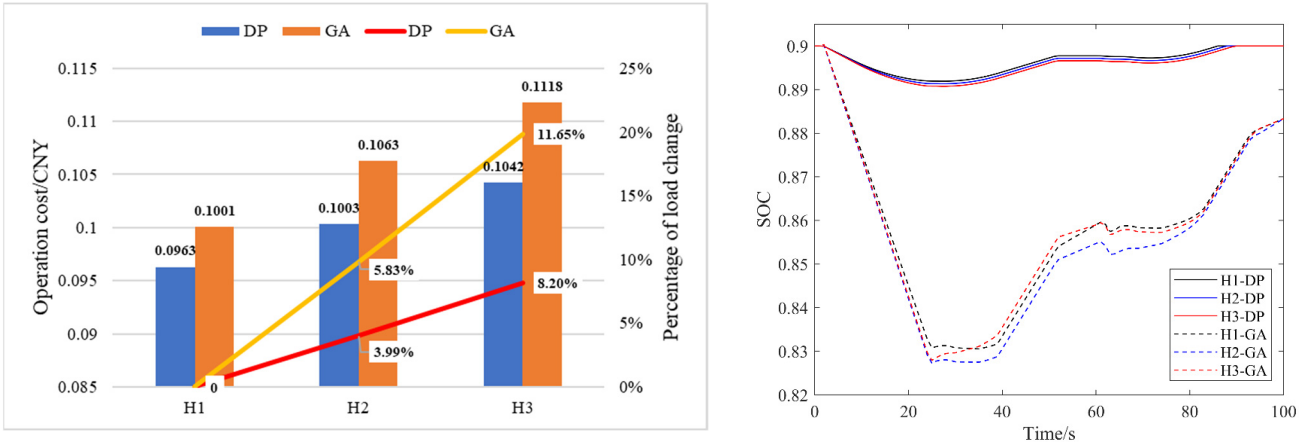


Figure 7. Operation cost (CNY) using different strategies. (The red font denotes the best results).

A similar upward trend is also evident in Figure 8a, with an increase in power demand. Specifically, the operation cost of the RTG crane using GAs experiences a substantial surge of approximately 5.83% or more, whereas the increase for DP is only 3.99%. These observations highlight that in scenarios involving heavy loads, such as in ports, the advantages of using DP are further emphasized. The variation in the SOC based on DP and GAs is shown in Figure 8b. The results indicate the lower power demands correlate with reduced changes in the SOC, as expected.



(**a**) (**b**)

Figure 8. The operation cost and variation in the SC SOC under different load profiles by DP and GA: (**a**) operation cost (CNY); (**b**) variation in SOC.

Therefore, in order to minimize operation cost under the volume limitations of the hydrogen tank, reducing $P_{fc\max}$ is feasible while satisfying the power demands. Similarly, the SC capacity configuration can also adopt the same strategy, where $P_{sc\max}$ only needs to satisfy the transient peak power demands during startup or acceleration. This configuration optimization can reduce the volume of the powertrain system and avoid resource waste. However, the prerequisite is that the power demands must be met; for example, the values in P6 cannot make the RTG crane operate normally.

6. Conclusions

This paper introduces a novel FC/SC hybrid powertrain system and a JO design integrated with a DP-based EMS strategy for RTG cranes in ports. The system is designed with the objectives of reducing carbon emission and minimizing operational cost, including equivalent hydrogen consumption and the FCS degradation cost, thereby addressing critical challenges in decarbonizing port equipment. The methodology employs a JO: preliminary parameterization based on standard handling cycles and a DP-based EMS targeting dual energy-economic optimization. An entire operating cycle and two representative operations were considered for verification. This study establishes a pioneering framework for hydrogen-powered port equipment. The core conclusions are summarized below:

1. The JO framework achieves dual energy-economic objectives, demonstrating through port validation a 57.33% fuel economy boost while reducing capacity redundancy of the SC by 12.7%.
2. As the first implementation of DP in fixed and heavy-load cycles of port cranes, this study provides optimal benchmark solutions for evaluating other EMSs. DP reduces operational costs by 5.47% and 12.50% compared to GAs and rule-based strategies, respectively, in the EOC.
3. In the process of the JO design, smaller values of $P_{fc\max}$ and C_{sc} can reduce operation cost and prevent resource waste while $P_{sc\max}$ only needs to satisfy the transient peak power demands during startup or acceleration. These findings aid FCRTG crane configuration design in ports.

For further research, the focal points will be centered on the following aspects:

1. A comprehensive mission profile and degradation of FCs will be systematically identified to ensure a thorough evaluation of the designed powertrain system for RTG cranes, yielding a solution with pan-scenario adaptability and balanced flexibility and efficiency performance.
2. DP is more suitable for offline computing and is limited in real-time EMS applications. Thus, a computationally efficient and feasible EMS should be developed to minimize operation costs for RTG cranes serving port container handling.

Author Contributions: Conceptualization, P.W. and J.D.; methodology, P.W.; software, Z.J.; validation, Z.N. and Z.J.; formal analysis, P.W.; investigation, Z.N.; resources, D.Z.; data curation, Z.N.; writing—original draft preparation, P.W.; writing—review and editing, J.D.; visualization, Z.N.; supervision, P.Y.; project administration, J.D.; funding acquisition, J.D. All authors have read and agreed to the published version of the manuscript.

Funding: This research is supported by the Key Research and Development Program Supported Project of Wuhan City (No. 2024010702030126) and the Jiangsu Special Equipment Safety Supervision and Inspection Research Institute (KJ(Y)2023035).

Data Availability Statement: Data will be made available on request.

Conflicts of Interest: Authors Pengcheng Yin and Danyang Zhao were employed by the company China Railway Siyuan Survey and Design Group Co., Ltd. The remaining authors declare that the research was conducted in the absence of any commercial or financial relationships that could be construed as a potential conflict of interest.

Appendix A

The equivalent circuits of the two DC/DC converters in different states along with the corresponding voltage and current waveforms are presented in the appendix.

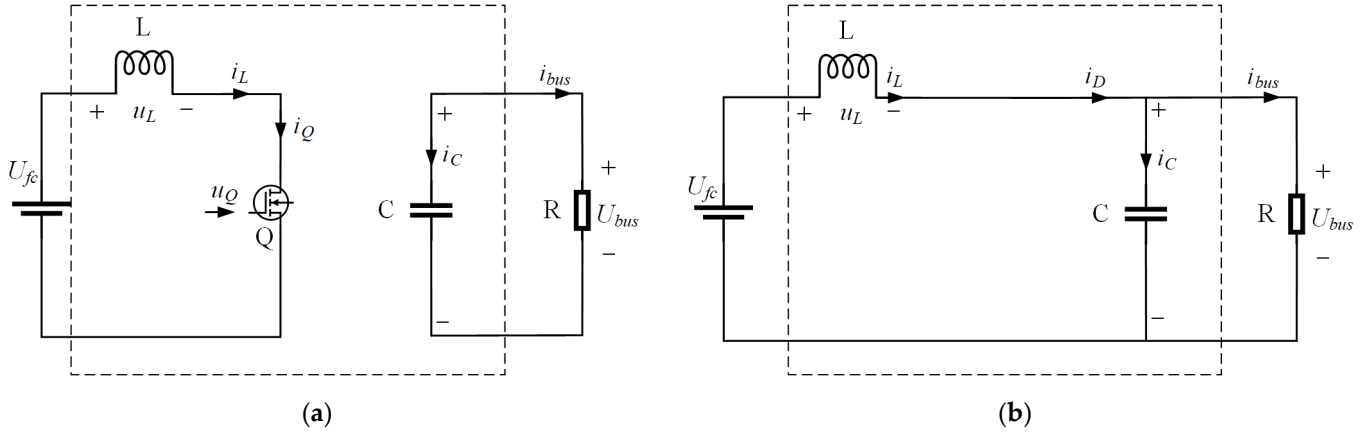


Figure A1. Two working states of the boost DC/DC converter: (**a**) the equivalent circuit during 0~T_{on}; (**b**) the equivalent circuit during T_{on}~T_s.

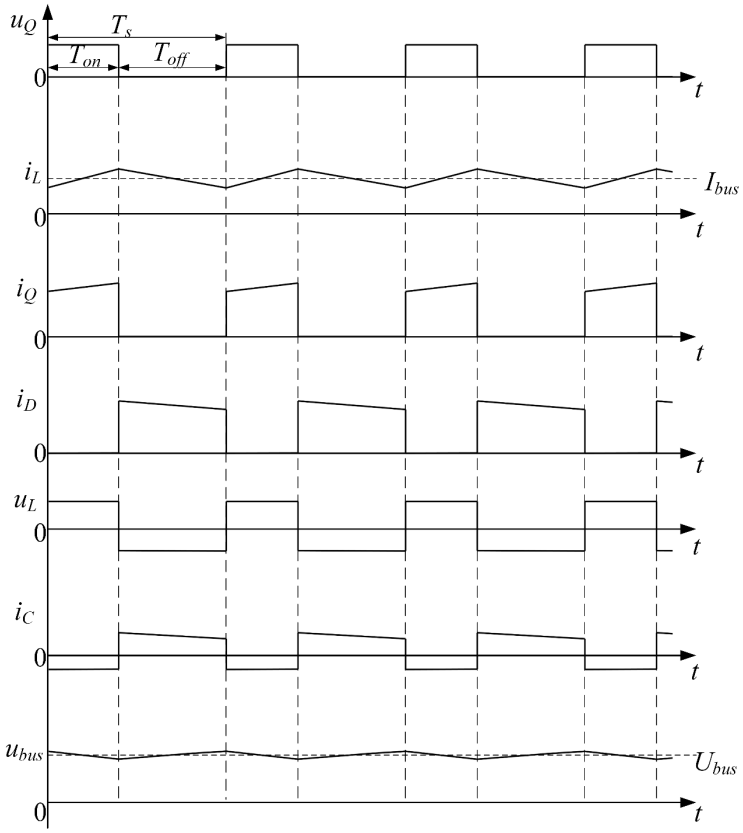


Figure A2. The voltage and current waveforms of the boost DC/DC converter.

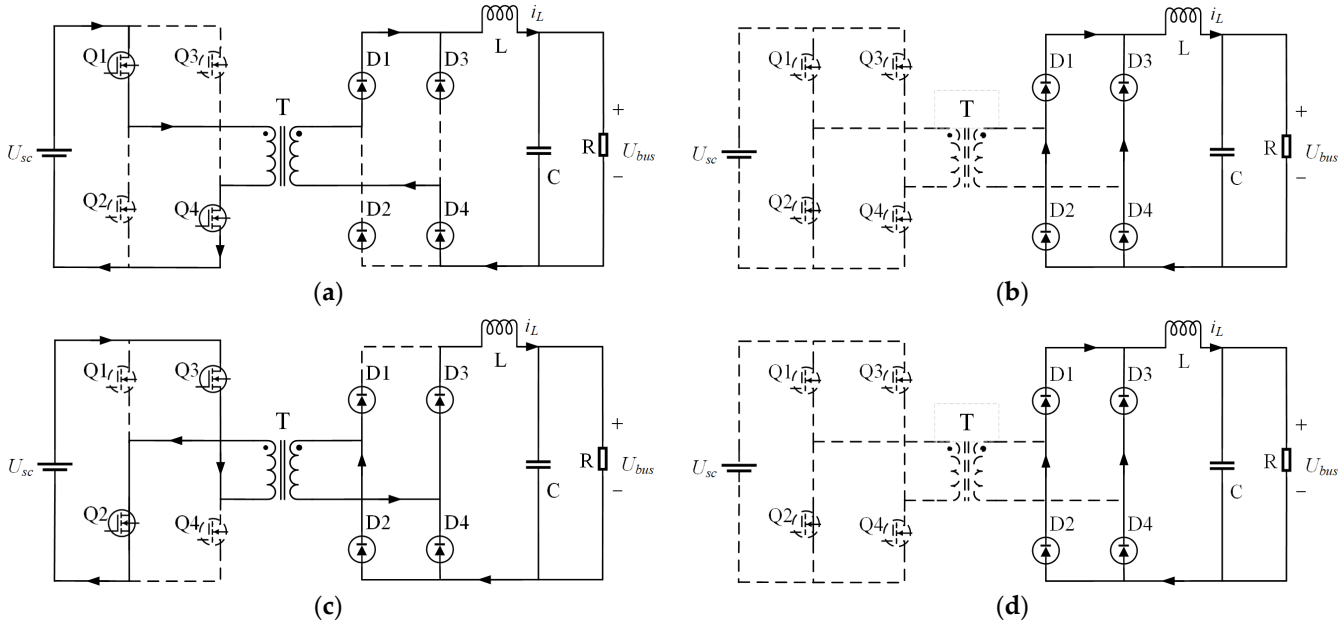


Figure A3. Four working states of the bidirectional full-bridge DC/DC converter (The dashed lines represent the partial disconnection of the circuit): (**a**) the equivalent circuit during T_0~T_1; (**b**) the equivalent circuit during T_1~T_2; (**c**) the equivalent circuit during T_2~T_3; (**d**) the equivalent circuit during T_3~T_4.

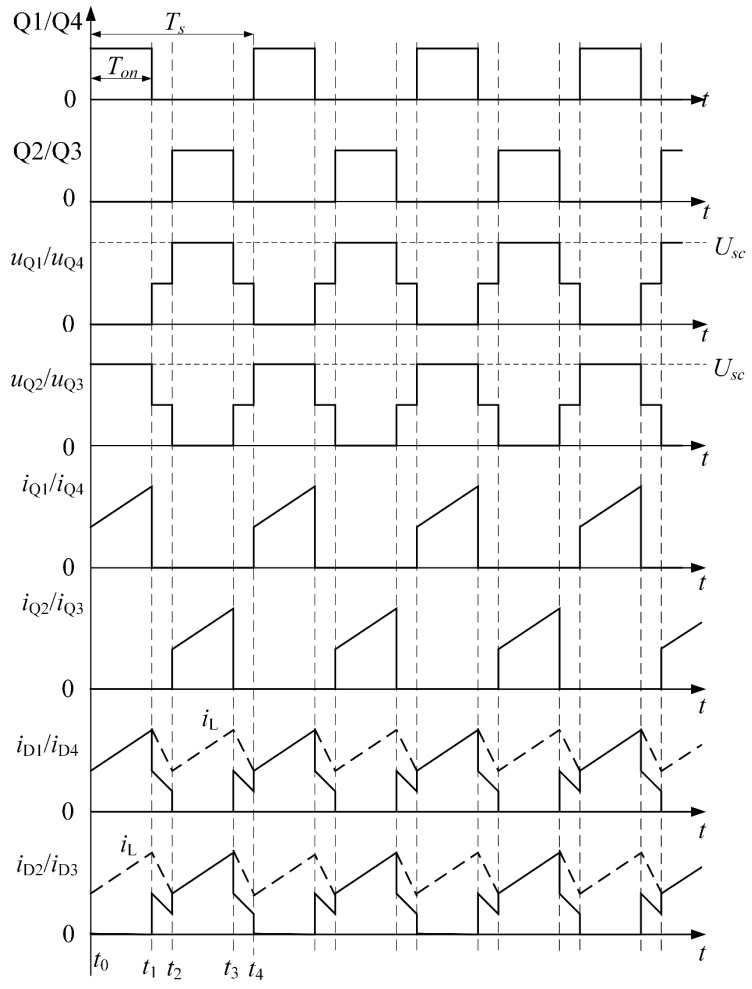


Figure A4. The voltage and current waveforms of the bidirectional full-bridge DC/DC converter.

References

1. Zhang, Q.; Tan, Z.Y.; Wang, S.A.; Zhen, L. Shore hydrogen deployment problem in green ports. *Comput. Oper. Res.* **2024**, *165*, 106585. [CrossRef]
2. Hu, M.; Dong, Y. China's shipping emissions governance: Status and prospects under the dual carbon goal. *Front. Mar. Sci.* **2024**, *11*, 1405312. [CrossRef]
3. Wang, P.Y.; Dou, J.P.; Su, W.S.; Jiang, Z.K.; Shi, Y.D. An energy management strategy based on dynamic programming for fuel cell hybrid trucks in ports. *Int. J. Hydrogen Energy* **2024**, *82*, 123–133. [CrossRef]
4. Kusakana, K. Optimal energy management of a retrofitted Rubber Tyred Gantry Crane with energy recovery capabilities. *J. Energy Storage* **2021**, *42*, 103050. [CrossRef]
5. Antonelli, M.; Ceraolo, M.; Desideri, U.; Lutzemberger, G.; Sani, L. Hybridization of rubber tired gantry (RTG) cranes. *J. Energy Storage* **2017**, *12*, 186–195. [CrossRef]
6. Wei, H.L.; Gu, W.; Chu, J.X. The dynamic power control technology for the high power lithium battery hybrid rubber-tired gantry (RTG) crane. *IEEE Trans. Ind. Electron.* **2019**, *66*, 132–140. [CrossRef]
7. Kusakaka, K.; Phiri, S.F.; Numbi, B.P. Optimal energy management of a hybrid diesel generator and battery supplying a RTG crane with energy recovery capability. *Energy Rep.* **2021**, *7*, 4769–4778. [CrossRef]
8. Takalani, R.; Masisi, L. Energy consumption optimization strategy for port cranes based on Pontryagin's minimum principle and filtering strategies. *IEEE Access* **2025**, *13*, 64991–65003. [CrossRef]
9. Boretti, A. Advancing sustainable mobility: Integrating flywheel kinetic energy recovery systems with high-efficiency hydrogen internal combustion engines. *Int. J. Hydrogen Energy* **2025**, *125*, 354–363. [CrossRef]
10. Ferrara, A.; Jakubek, S.; Hametner, C. Cost-optimal design and energy management of fuel cell electric trucks. *Int. J. Hydrogen Energy* **2023**, *48*, 16420–16434. [CrossRef]
11. Shen, Y.P.; Xie, J.C.; He, T.; Yao, L.; Xiao, Y.Q. CEEMD-fuzzy control energy management of hybrid energy storage systems in electric vehicles. *IEEE Trans. Energy Convers.* **2024**, *39*, 555–566. [CrossRef]
12. Chen, B.; Ma, R.Q.; Zhou, Y.; Ma, R.; Bai, H.; Jiang, W.T.; Zhang, Z.; Xun, Q. A universal cost-oriented powertrain component size design scheme using nested framework for fuel cell trucks. *Energy Convers. Manag.* **2025**, *327*, 119521. [CrossRef]
13. Liu, J.L.; Chun, E.; Jin, X.M.; Zhang, H.; Liu, J.L.; Wang, Z.R. Combustion and fire risk evolution of low-temperature aged lithium-ion batteries. *J. Energy Storage* **2026**, *159*, 121613. [CrossRef]
14. Chen, L.; Wang, Z.X.; Yi, W.; Zhang, Y.; Fu, Y.X. Bus Voltage Fluctuation Suppression Strategy for Hybrid Energy Storage Systems Based on MPC Power Allocation and Tracking. *Electronics* **2025**, *14*, 3390. [CrossRef]
15. Corral-Vega, P.J.; Fernández-Ramírez, L.M.; García-Triviño, P. Hybrid powertrain, energy management system and techno-economic assessment of rubber tyre gantry crane powered by diesel-electric generator and supercapacitor energy storage system. *J. Power Sources* **2019**, *412*, 311–320. [CrossRef]
16. Jia, C.C.; Liu, W.; He, H.W.; Chau, K.T. Health-conscious energy management for fuel cell vehicles: An integrated thermal management strategy for cabin and energy source systems. *Energy* **2025**, *333*, 137330. [CrossRef]
17. You, J.H.; Wu, J.L.; Zhang, Y.Q.; Shi, W.L. Optimization of fuel cell heavy-duty commercial vehicles sizing and energy management based on an offline-online framework. *J. Power Sources* **2026**, *666*, 14. [CrossRef]
18. Ramos, G.A.; de Pérez-Cabrero, T.M.; Domènech-Mestres, C.; Costa-Castelló, R. Industrial Robots Fuel Cell Based Hybrid Power-Trains: A Comparison between Different Configurations. *Electronics* **2021**, *10*, 1431. [CrossRef]
19. Bulak, M.E. A frontier approach to eco-efficiency assessment in the world's busiest sea ports. *Sustainability* **2024**, *16*, 1142. [CrossRef]
20. Bloemert, P.; Saraceni, A. European ports transition to carbon-neutral energy: A multiple regression analysis. *Transp. Res. Interdiscip. Perspect.* **2024**, *27*, 101187. [CrossRef]
21. Zhao, X.L.; Wang, L.; Zhou, Y.L.; Pan, B.X.; Wang, R.C.; Wang, L.M.; Yan, X.Q. Energy management strategies for fuel cell hybrid electric vehicles: Classification, comparison, and outlook. *Energy Convers. Manag.* **2022**, *270*, 116179. [CrossRef]
22. Lamedica, R.; Ruvio, A.; Palagi, L.; Mortelliti, N. Optimal siting and sizing of wayside energy storage systems in a dc railway line. *Energies* **2020**, *13*, 6271. [CrossRef]
23. Lu, D.G.; Yi, F.Y.; Hu, D.H.; Li, J.W.; Yang, Q.Q.; Wang, J. Online optimization of energy management strategy for FCV control parameters considering dual power source lifespan decay synergy. *Appl. Energy* **2023**, *348*, 121516. [CrossRef]
24. Jia, C.C.; Zhou, J.M.; He, H.W.; Li, J.W.; Wei, Z.B.; Li, K.A. Health-conscious deep reinforcement learning energy management for fuel cell buses integrating environmental and look-ahead road information. *Energy* **2024**, *290*, 130146. [CrossRef]
25. Tang, X.W.; Shi, L.; Zhang, Y.J.; Li, B.B.; Xu, S.C.; Song, Z.Y. Degradation adaptive energy management strategy for FCHEV based on the rule-DDPG method: Tailored to the current SOH of the powertrain. *IEEE Trans. Transp. Electrif.* **2025**, *11*, 993–1003. [CrossRef]

26. Muniandi, B.; Wan, S.Y.; El-Yabroudi, M. Bi-Directional Charging with V2L Integration for Optimal Energy Management in Electric Vehicles. *Electronics* **2024**, *13*, 4221. [CrossRef]
27. Sipra, A.T.; Azeem, F.; Memon, Z.A.; Baig, S.; Jaffery, M.H. Design and assessment of energy management strategy on rail coaches using solar PV and battery storage to reduce diesel fuel consumption. *Energy* **2024**, *288*, 129718. [CrossRef]
28. Xu, Z.; Zhao, N.; Yan, Y.; Gao, S.G.; Hillmansen, S. Electric-thermal collaborative system and control for hydrogen-fuel cell passenger trains in the UK's winter. *Energy Convers. Manag.* **2025**, *328*, 119629. [CrossRef]
29. Varlese, C.; Ferrara, A.; Hametner, C.; Hofmann, P. Experimental validation of a predictive energy management strategy for agricultural fuel cell electric tractors. *Int. J. Hydrogen Energy* **2024**, *77*, 1–14. [CrossRef]
30. Radrizzani, S.; Panzani, G.; Trezza, L.; Pizzocaro, S.; Savaresi, S.M. An add-on model predictive control strategy for the energy management of hybrid electric tractors. *IEEE Trans. Veh. Technol.* **2024**, *73*, 1918–1930. [CrossRef]
31. Radrizzani, S.; Panzani, G.; Savaresi, S.M. Simultaneous energy management and speed control in a hybrid tractor with experimental validation. *IEEE Trans. Control Syst. Technol.* **2024**, *32*, 1285–1297. [CrossRef]
32. Haffaf, A.; Lakdja, F. Comprehensive multi-stage 3E feasibility and overall sensitivity analysis of PV-Diesel-BESS hybrid on/off grid system under various battery technologies, energy controls strategies, and solar tracking techniques. *Energy Convers. Manag.* **2024**, *312*, 37. [CrossRef]
33. Wang, S.F.; Tan, Q.J.; Ding, X.Y.; Li, J. Efficient microgrid energy management with neural-fuzzy optimization. *Int. J. Hydrogen Energy* **2024**, *64*, 269–281. [CrossRef]
34. Ahmed, D.; Ebeed, M.; Ali, A.; Alghamdi, A.S.; Kamel, S. Multi-Objective Energy Management of a Micro-Grid Considering Stochastic Nature of Load and Renewable Energy Resources. *Electronics* **2021**, *10*, 403. [CrossRef]
35. Song, K.; Huang, X.; Xu, H.J.; Sun, H.; Chen, Y.H.; Huang, D.Y. Model predictive control energy management strategy integrating long short-term memory and dynamic programming for fuel cell vehicles. *Int. J. Hydrogen Energy* **2024**, *56*, 1235–1248. [CrossRef]
36. Gharibeh, H.F.; Yazdankhah, A.S.; Azizian, M.R. Energy management of fuel cell electric vehicles based on working condition identification of energy storage systems, vehicle driving performance, and dynamic power factor. *J. Energy Storage* **2020**, *31*, 101760. [CrossRef]
37. Lü, X.Q.; He, S.J.; Xu, Y.Z.; Zhai, X.R.; Qian, S.C.; Wu, T.; Wangpei, Y.Q. Overview of improved dynamic programming algorithm for optimizing energy distribution of hybrid electric vehicles. *Electr. Power Syst. Res.* **2024**, *232*, 110372. [CrossRef]
38. Takalani, R.; Masisi, L. Development of an energy management strategy for port cranes. In Proceedings of the 47th Annual Conference of the IEEE-Industrial-Electronics-Society (IECON), Toronto, ON, Canada, 13–16 October 2021; pp. 1–6. [CrossRef]
39. Chen, D.W.; Niu, W.Q.; Gu, W.; Schofield, N. Game-based energy management method for hybrid RTG cranes. *Energies* **2019**, *12*, 3589. [CrossRef]
40. Alasali, F.; Haben, S.; Holderbaum, W. Stochastic optimal energy management system for RTG cranes network using genetic algorithm and ensemble forecasts. *J. Energy Storage* **2019**, *24*, 100759. [CrossRef]
41. Lin, S.M.; Zhen, L.; Wang, W.C. Planning low carbon oriented retrofit of diesel-driven cranes to electric-driven cranes in container yards. *Comput. Ind. Eng.* **2022**, *173*, 108681. [CrossRef]
42. Liu, H.A.; Jiang, J.; Zhan, S.; Yang, X.Y.; Yu, D.M.; Yan, G.G. Study on energy management model of integrated New Energy-Storage-Charging system considering the influence of uncertainties. *Fuel* **2023**, *331*, 125784. [CrossRef]
43. Alasali, F.; Haben, S.; Becerra, V.; Holderbaum, W. Optimal Energy Management and MPC Strategies for Electrified RTG Cranes with Energy Storage Systems. *Energies* **2017**, *10*, 1598. [CrossRef]
44. Razmjooy, N. A survey on parameters estimation of the proton exchange membrane fuel cells based on the swarm-inspired optimization algorithms. *Front. Energy Res.* **2023**, *11*, 1148323. [CrossRef]
45. Rudolf, T.; Schurmann, T.; Schwab, S.; Hohmann, S. Toward holistic energy management strategies for fuel cell hybrid electric vehicles in heavy-duty applications. *Proc. IEEE* **2021**, *109*, 1094–1114. [CrossRef]
46. Di Ilio, G.; Di Giorgio, P.; Tribioli, L.; Bella, G.; Jannelli, E. Preliminary design of a fuel cell/battery hybrid powertrain for a heavy-duty yard truck for port logistics. *Energy Convers. Manag.* **2021**, *243*, 114423. [CrossRef]
47. Liu, Y.F.; Li, M.C.; Wang, Y.J.; Sun, Z.D.; Chen, Z.H. Predictive Energy Management for Fuel Cell Hybrid Vehicles Considering Efficiency and Safety. *IEEE Trans. Power Electron.* **2024**, *39*, 13842–13852. [CrossRef]
48. Zhou, Y.; Ravey, A.; Péra, M.C. Real-time cost-minimization power-allocating strategy via model predictive control for fuel cell hybrid electric vehicles. *Energy Convers. Manag.* **2021**, *229*, 18. [CrossRef]
49. Naseri, F.; Karimi, S.; Farjah, E.; Schaltz, E. Supercapacitor management system: A comprehensive review of modeling, estimation, balancing, and protection techniques. *Renew. Sust. Energ. Rev.* **2022**, *155*, 111913. [CrossRef]
50. Mounika, K.; Bhattacharjee, A. Design and experimental validation for performance analysis of non-isolated power converter topologies in fuel cell integrated dynamic load based local energy systems. *Energy* **2025**, *322*, 28. [CrossRef]
51. Papaioannou, V.; Pietrosanti, S.; Holderbaum, W.; Becerra, V.M.; Mayer, R. Analysis of energy usage for RTG cranes. *Energy* **2017**, *125*, 337–344. [CrossRef]

52. Corral-Vega, P.J.; García-Triviño, P.; Fernández-Ramírez, L.M. Design, modelling, control and techno-economic evaluation of a fuel cell/supercapacitors powered container crane. *Energy* **2019**, *186*, 115863. [CrossRef]
53. Zhang, X.; Fu, G.T.; Liao, Q.; Tu, R.F.; Zhang, H.R.; Liang, Y.T. Large-scale hydrogen supply chain vision with blended pipeline transportation of China. *Renew. Energy* **2025**, *240*, 122230. [CrossRef]
54. He, Y.N.; Liu, J.X.; Deng, X.Y.; Zhang, Y.H.; Ma, T. Optimal design of a hydrogen supply chain taking into account economic costs, energy consumption, and carbon emissions-A case study of Shanghai, China. *Int. J. Hydrogen Energy* **2024**, *94*, 795–805. [CrossRef]

Disclaimer/Publisher's Note: The statements, opinions and data contained in all publications are solely those of the individual author(s) and contributor(s) and not of MDPI and/or the editor(s). MDPI and/or the editor(s) disclaim responsibility for any injury to people or property resulting from any ideas, methods, instructions or products referred to in the content.